Selective Photocatalytic Oxidation of 5-Hydroxymethylfurfural to 2,5-Furandicarboxaldehyde by Polymeric Carbon Nitride-Hydrogen Peroxide Adduct

M. Ilkaeva,[a] I. Krivtsov,[*a,b] E.I. García-López,[c] G. Marcì,[c] O. Khainakova,[a] J.R. García,[a] L. Palmisano,[c] E. Díaz,[d] S. Ordóñez[d.]

[a] Departments of Organic and Inorganic Chemistry, Physical and Analytical Chemistry, University of Oviedo-CINN, 33006 Oviedo, Spain.

[b] Nanotechnology Education and Research Center, South Ural State University, 454080 Chelyabinsk, Russia.

[c] "Schiavello-Grillone" Photocatalysis Group. Dipartimento di Energia, Ingegneria dell'informazione e modelli Matematici (DEIM), Università di Palermo, Viale delle Scienze, 90128 Palermo, Italy.

[d] Department of Chemical and Environmental Engineering, University of Oviedo, 33006 Oviedo, Spain.

Corresponding author e-mail: krivtsovigor@uniovi.es; Tel: +34 985 103 030

Abstract

Polymeric carbon nitride-hydrogen peroxide adduct ($PCN-H_2O_2$) has been prepared, thoroughly characterised and its application for selective photocatalytic conversion of 5-hydroxymethylfurfural (HMF) to 2,5-furandicarboxaldehyde (FDC) in aqueous suspension has been studied. The $PCN-H_2O_2$ adduct is stable in aqueous suspension under UV and solar irradiation up to 100 °C. It is also stable up to 200 °C if heated in air, while at temperatures close to 300 °C its decomposition takes place. Based on the obtained characterisation data it has been proposed that H_2O_2 attaches to the non-polymerised carbon nitride species and to the heptazine nitrogen atoms, thus producing strong hydrogen bonding within the $PCN-H_2O_2$ adduct. The blockage of the surface amino-groups in $PCN-H_2O_2$ by H_2O_2 hinders the interaction of HMF with these sites, which are responsible for unselective substrate conversion. $PCN-H_2O_2$ possesses a superior selectivity in natural solar light assisted oxidation of HMF to FDC reaching 80% with respect to its thermally etched PCN counterpart, which gives rise to a 40-50% selectivity. We believe that the exceptional performance of the applied photocatalyst in the selective photocatalytic conversion of HMF to a high added value FDC in a green solvent under natural illumination makes a significant contribution to the development of environmentally friendly technologies for biomass valorisation.

Keywords: photocatalysis; carbon nitride; selective photo-oxidation; 5-hydroxymethylfurfural; 2,5-furandicarboxaldehyde.

Introduction

Wood industry and agricultural sector release a large amount of by-products and wastes, which if processed appropriately, can be converted into a range of valuable chemicals or fuels. This renewable feedstock known under the general term "biomass", despite being used for multiple purposes, is still in the spotlight of the research community, inasmuch as newly emerged technologies allow benefiting from its more complete use. Cellulose, an abundant biomass compound, can be upgraded by undergoing hydrolysis producing hexose sugars, which after being subsequently dehydrated give a biomass platform molecule 5-hydroxymethyl furfural (HMF) [1,2]. While HMF itself has few applications, the products of its oxidation 2,5-furandicarboxylic acid (FDCA) and 2,5-diformylfuran, also known as 2,5-furandicarboxaldehyde (FDC), possess properties making them valuable for biopolymer production [3-7]. Many catalytic procedures have been developed for obtaining both FDCA [8,9] and FDC [9-14] by oxidising HMF, but photocatalysis is among the most economic and greener alternatives as it benefits from a nearly free energy source, which is solar radiation, and does not require toxic oxidants. The outburst of interest toward semiconductor-assisted selective photo-oxidation has already resulted in an impressive number of exhaustive reviews on mechanisms and applied aspects of this process [15-20]. Light-initiated transformation of biomass aiming to produce fuel has recently been reported by Wakerley et al. [21], while the approaches for its chemical upgrading has been reviewed in [22-23].

HMF itself was subjected to electrophotocatalytic [24] and photocatalytic conversion in aqueous phase using TiO_2 as the photocatalyst, and FDC was found to be the main oxidation product of this reaction [25,26]. Although TiO_2, and especially N-doped TiO_2 promoted the formation of FDC from HMF, the selectivity of this process was low reaching 30% for the best photocatalysts, owing to formation on the TiO_2 surface of highly oxidative hydroxyl radicals inducing the substrate mineralisation [26]. Obviously, an alternative material for such transformation was in demand. It has not been long since polymeric carbon nitride (PCN) (the recommended term for graphitic carbon nitride, $g-C_3N_4$) [27] photocatalyst has emerged [28]. In addition to its high ability to reduce water protons to molecular hydrogen, it possesses a valence band (VB) potential which does not permit direct water oxidation to $^\bullet OH$ radicals [28], hence reducing the presence of notoriously unselective oxidative species in a water suspension of photocatalysts with organic

compounds. Despite this attractive property, this material has mostly been used for conversion of aromatic alcohols [29-32] and hydrocarbons [33-36] in organic solvents, while reports on its performance in aqueous phase are scarce [37-38]. Recently, the enhanced selectivity of PCN for aqueous phase HMF to FDC photo-oxidation with respect to that previously achieved in the presence of TiO_2 [25] has been reported [39-40]. A detrimental effect of the presence of non-polymerised carbon nitride species on the selectivity of photo-oxidation has also been observed [39]. Thermal etching applied to bulk PCN, principally with the purpose of increasing its specific surface area (SSA), also eliminated excessive NH and NH_2 moieties from the PCN surface resulting in the growth of selectivity toward the FDC production from 30% to 50% under solar irradiation [39]. The importance of controlling the interaction of substrate with the surface functional groups of PCN was even more stressed for chemoselective C–H bond oxidation of alkylphenolethoxylate molecules [41]. In this paper, we report the application of the PCN-H_2O_2 adduct for highly selective photocatalytic oxidation of HMF to FDC in aqueous medium under both UV and natural solar light irradiation.

Experimental Section

Materials

Melamine (99%), 30 wt% hydrogen peroxide water solution, 5-hydroxymethylfurfural (HMF) (≥99%), 2,5-furandicarboxyaldehyde (FDC) (≥99%), and 5-formyl-2-furoic acid (FFA) (≥99%) were purchased from Aldrich.

Synthesis

The bulk PCN was prepared via the thermal condensation method using melamine as the precursor according to the procedure described by Wang et al. [42]. Briefly, 10 g of melamine was placed in a covered ceramic crucible and heated in a muffle furnace at 2 °C min^{-1} up to 520 °C. Once the temperature was reached it was left for 2 h and slowly cooled down afterwards. By this procedure, 6 g of PCN was obtained. Bulk PCN was then subjected to thermal etching as previously reported [39,43], in order to produce high SSA PCN. For this purpose, 6 g of the bulk carbon nitride was powdered in a mortar, evenly spread on the bottom of a ceramic bowl with a diameter of 12 cm, heated in a static air atmosphere at 500 °C by using a temperature ramp of 3

°C min^{-1} and maintained for 4 h at the reached temperature before being cooled down. This procedure yielded 2.8 g of the thermally etched PCN sample, designated as **TE**. Finally, the PCN-H$_2$O$_2$ adduct, whose preparation and characterisation were reported elsewhere [41], was synthesized. For this, 2.8 g of **TE** was stirred in 50 mL of H$_2$O$_2$ aqueous solution (30 wt%) in an open beaker while heating at 70 °C until complete evaporation of the liquid was achieved. The obtained solid was washed thoroughly with deionized water, until H$_2$O$_2$ was no longer detected in the washing liquid, filtered and finally dried at 80 °C for 24 h giving the PCN-H$_2$O$_2$ adduct (**TEO**). After that, aliquots of the **TEO** sample, 0.87 g in each case, were treated at 200, 300, and 400 °C in air for 2 h, and the resulting samples were coded as **TEOx**, where "*x*" indicated the treatment temperature. For the sake of comparison, two more samples were synthesized. Thermally etched **TEO450** was prepared by treating the **TEO** sample at 450 °C in air. H$_2$O$_2$ modification of **TE** was also carried out using reflux treatment at 70 °C (**TEO_R**). Melamine-hydrogen peroxide adduct (**MHP**) was prepared and used as the reference for the assignment of carbon nitride surface species formed after the reaction with hydrogen peroxide. For this purpose, 10 g of melamine was mixed with 50 mL of 30 wt% H$_2$O$_2$ and let stirring while heated at 70 °C until the solvent was evaporated. The obtained solid was dried at 70 °C for 24 h.

Characterisation

Powder XRD patterns were registered in an X'pert PANanalytical diffractometer, using a Ni-filtered Cu-Kα radiation source and PixCel1D (tm) detector. Infrared spectra of the samples were recorded with 4 cm^{-1} resolution using an ATR module of a Varian 620-IR spectrometer. The surface elemental composition of the PCN and PCN-H$_2$O$_2$ samples, their valence band (VB) potentials, and the binding energies of C, N and O were measured by X-ray photoelectron spectroscopy (XPS) on a SPECS system equipped with a Hemispherical Phoibos analyser operating in a constant pass energy, using MgKα radiation (h·ν = 1253.6 eV). The absence of C–C bonds in carbon nitride made possible taking a signal of adventitious carbon at 284.8 eV as a reference. The elemental composition was estimated from the deconvoluted high-resolution data as to remove the contribution of adventitious carbon. The value of conduction band potential of the PCN samples was estimated by subtracting the value of band gap energy (BG) from that of the valence band energy (VB). The solid-state ^{13}C, ^{1}H MAS NMR, and ^{1}H-^{13}C CPMAS NMR spectra

were registered at the spinning rates of 5 kHz for ^{13}C, and 8 kHz for the other measurements using a Bruker Avance III 400WB spectrometer. A Shimadzu UV-2401 PC spectrophotometer equipped with an integrated sphere was used to obtain diffusive reflectance spectra (DRS) from the prepared samples supported on $BaSO_4$ pellets. The BG was estimated by applying the Kubelka-Munk function to the DRS data considering PCN as an indirect semiconductor. Photoluminescence spectra were recorded for the obtained materials by means of a standard spectrofluorimeter Edinburgh Instruments FLSP920 equipped with a 450 W Xe lamp as an excitation source (365 and 455 nm wavelengths were selected for the samples excitation). A Micromeritics ASAP 2020 was used to obtain adsorption-desorption isotherms of N_2 at 77 K. Specific surface area (SSA) was calculated from the nitrogen adsorption data by BET equation. Before the experiment, the samples were outgassed under vacuum at 200 °C. The temperature programmed desorption mass-spectroscopic (TPD-MS) analysis was carried out with help of a Micromeritics Autochem II 2920 system coupled with a ThermoStar mass spectrometer. For the analysis, 100 mg of a powdered PCN was put onto a fibreglass support inside a quartz U-tube, purged for 60 min with argon gas flowing through the sample at the rate of 10 mL min^{-1} at 35 °C and then heated at 10 °C min^{-1} up to 400 °C. The concentration of H_2O_2 released into water suspension by the PCN-H_2O_2 adduct was estimated photocolourimetrically by using titanium oxysulfate based method.

Photocatalytic oxidation of HMF

Partial photocatalytic oxidation of HMF to FDC under UV-light was carried out by using the experimental set-up described elsewhere [39]. A water-cooled Pyrex reactor containing 150 mL of aqueous suspension was irradiated with six Actinic BL TL MINI 15 W/10 Philips fluorescent lamps having an irradiation maximum at 365 nm. The initial HMF concentration was 0.5 mM at the natural pH if not stated otherwise. The amount of solid photocatalyst used for the experiments was 100 mg. In this way, all the entering photons were virtually absorbed by the suspension. The impinging radiation energy in the range 315–400 nm was measured by a radiometer Delta Ohm DO9721 with a UVA probe and its average value was 3.9 W m^{-2}. The performance of the most efficient photocatalyst (**TEO**) was tested in a series of three consecutive reaction runs. The suspension of **TEO** was left for 24 h to separate the photocatalyst after the photocatalytic

reaction. Then, the limpid solution was removed, 150 mL of fresh HMF 0.5 mM solution was introduced into the reactor and the test was repeated. Samples of the irradiated solution were withdrawn at fixed time intervals and immediately filtered through 0.25 μm membranes (polypropylene, VWR) to separate the photocatalyst particles. Liquid aliquots were analysed by a Thermo Scientific Dionex UltiMate 3000 HPLC equipped with a Diode Array detector and a REZEK ROA organic acid H^+ column with aqueous 2.5 mM H_2SO_4 solution mobile phase at a flow rate of 0.6 mL min^{-1}. The concentrations of HMF, FDC and FFA were determined. Standards purchased from Sigma-Aldrich with a purity >99% were used to identify the products formed during the reaction and to obtain the calibration curves.

The photocatalytic reactions under natural solar irradiation were carried out on clear sunny days from March to May in Palermo (Italy) from 9:30 to 13:30. Typically, 75 mL of 0.5 mM HMF solution and 50 mg of the PCN or PCN-H_2O_2 samples were introduced into a round-shaped Pyrex batch reactor having a total volume of 125 mL and a diameter of 10 cm. Additionally, the **TEO** sample was tested under the same conditions, but at initial HMF concentrations of 1mM and 2 mM. The suspensions of the PCN samples in HMF solution were continuously magnetically stirred and probes of approximately 2.5 mL were withdrawn every 30 min and analysed by using the previously described analytical procedure. The photon flux in the range of 315-400 nm, which largely determines the reactivity of PCN under present conditions [39], was measured every 10 min throughout the photocatalytic runs, and the cumulative energy (E) was estimated based on the obtained data. The E value allows the comparison of photoreactivity results obtained under natural sunlight irradiation at different meteorological conditions. It is given by:

$$E = \int_0^t I(t)\,dt \tag{1}$$

in which "I(t)" is the instantaneous photon flow and "t" the irradiation time. The values of "I(t)" were calculated from the recorded values of irradiance, UVG(t), by using the following relationship:

$$I(t) = UVG(t)\cdot S \tag{2}$$

in which "S" is the total irradiated surface and "UVG" is the irradiance (in the 315-400 nm wavelength range) [44].

The detection of hydroxyl radicals was carried out by a standard terephthalic acid (TA) method [45]. For this, 12 mg of PCN was suspended in 150 mL of 3 M solution of TA in 0.01 M of

NaOH. The suspension was irradiated in the same set-up described above, the samples were withdrawn at fixed time intervals and PL spectra of the formed hydroxyterephthalic acid were recorded at excitation wavelength of 310 nm.

Results and Discussion

XRD and FTIR

According to the XRD patterns of the thermally etched PCN and the PCN-H_2O_2 adduct samples shown in Figure 1, the typical for PCN reflections of (002), (100), and (101) planes are observed. Noteworthy, the full-width at half-maximum (FWHM) of the diffraction peak at 27.7º (2θ) is decreased to 1.46° for the **TEO** sample with respect to that of **TE** (1.66°), indicating the change in preferential orientation or bonding in the adduct, also noted elsewhere [41] (Fig. 1 inset). This finding differs from other works reporting the use of H_2O_2 for hydrothermal carbon nitride treatment, where harsh conditions favoured exfoliation of PCN, consequently reducing the intensity of diffraction maxima [46,47]. Thermal treatment at 200 and 400 °C applied to the **TEO** sample does not lead to further changes of FWHM of the (002) peak, which is maintained in the range of 1.40° to 1.46° (Fig. 1 inset). For the PCN-H_2O_2 subjected to 400 °C (**TEO400**) a shift of the peak position is clearly seen on the XRD pattern of this sample (Fig. 1 inset), implying that thermal etching has already taken place at 400 °C [48].

FIGURE 1

FTIR study is in agreement with the discussed XRD results, as it confirms that no major changes in polymeric C_3N_4 structure occur neither after the reaction with H_2O_2 nor after the subsequent heating (see Electronic Supplementary Information, Fig. S1). The range of wavenumbers from 1100 to 1700 cm^{-1} is typical of C–N stretching vibrations in heptazine heterocycles (Fig. S1), and it remains almost identical whatever treatment is applied to the **TE** or **TEO** samples.

XPS study

The C 1s XPS spectra (Fig. S2) show that the positions of the corresponding maxima do not change and the profiles of the spectra are not significantly modified after the applied treatment. The XPS probing of the N 1s region results in a broad maximum, which can be deconvoluted into the three major contributions from C–N=C (N1), N–(C)$_3$ (N2) and C–N–H (N3) species (Fig. S3).

The ratio of N1 to N3 remains nearly constant for all the samples, whereas it is not the case of the N1/N2 ratio (Table S1). Due to the significant peak width and the possible superposition of the signals from several N-containing moieties, it is difficult to unambiguously attribute the observed changes to certain groups in PCN-H_2O_2. However, one can suggest that the decrease of the N1 to N2 ratio for **TEO** is a consequence of the enhanced condensation degree of PCN, while the following changes manifested by the samples subjected to thermal treatment at 200 and 300 °C result most likely from the reaction of evolving hydrogen peroxide with carbon nitride (Table S1). In accordance with the previously reported data [41], XPS results show the increased surface oxygen content in **TEO** contrary to its unmodified counterpart, the **TE** sample (Table 1). Interestingly, the concentration of surface oxygen decreases slightly after the material is heated at 200 °C, but it drops down, even below the value obtained for **TE,** in the samples heated up to 300 and 400°C (Table 1).

TABLE 1

FIGURE 2

The nature of the oxygen-containing species in the PCN-H_2O_2 samples is determined from the O 1s XPS spectra. It appears that the peak of O 1s, centred at 532.5 eV for the **TE** sample, is displaced to 531.6 eV for **TEO** (Fig. 2). The position of the peak remains unchanged even after the PCN-H_2O_2 adduct is heated up to 300 °C. The XPS spectrum of **TEO400** clearly indicates that the O 1s maximum returns to the same value of binding energy as that of the starting material (Fig. 2). The similar shift of the O 1s peak was earlier reported for H_2O_2-treated carbon nitrides [46,47], however, the assignment of these oxygen-containing moieties is a controversial matter. Li et al. [47], who subjected PCN to hydrothermal treatment in H_2O_2 solution, attributed the appearance of the peak at 531.6 eV to the formation of N–C–O or adsorbed O_2 species. Liu et al. [46] suggested that the cause was an O-doping of the heptazine skeleton. The absence of any noticeable changes in the chemical states of C and N atoms in the PCN-H_2O_2 samples prepared in this work compared to the thermally etched PCN, and the fact that the adsorbed oxygen is expected to appear in XPS spectra at about 532 eV [49] suggest to hold on to the earlier proposed hypothesis [41]. The reaction of melamine with hydrogen peroxide produces the crystalline **MHP** adduct [50,51], whose structure is reported by Chernyshov et al. [52]. In a very similar way, H_2O_2 can interact with the surface carbon nitride species [41]. Here, we corroborate this hypothesis by

comparing the O 1s XPS data obtained for the crystalline **MHP** complex, whose structure is confirmed by the XRD measurement (Fig. S4), and the PCN-H_2O_2 samples (Fig. 2). The O 1s peak of **MHP** complex is centred at 531.3 eV nearly coinciding with the O 1s maximum found for the **TEO**, **TEO200**, and **TEO300** samples; however, the contribution of other oxygen species also present in PCN causes its shift to 531.5–531.6 eV (Fig. 2, Table 1). A drastic reduction of the oxygen content observed for **TEO300** can be attributed to the elimination of a greater part of bonded H_2O_2, although the fact that the position of the O 1s maximum remains unchanged could indicate the presence of small quantities of H_2O_2 retained in the material. Thus, considering the surface elemental composition and the position of the O 1s maximum, one can conclude that the reaction of PCN with H_2O_2 produces a PCN-H_2O_2 adduct stable in air up to 200 °C.

Solid-state MAS ^{1}H, ^{13}C, and ^{1}H-^{13}C CPMAS NMR studies

The chemical shifts of the two maxima at 156.7 and 165.0 ppm on the ^{13}C MAS NMR spectra correspond to carbon atoms bonded to three nitrogen atoms of the aromatic carbon nitride structural units (C_i) and to those bearing non-polymerised NH_2 and partially polymerised NH fragments (C_e), respectively (Fig. 3, Fig. 4A). This is confirmed by the ^{1}H-^{13}C CPMAS NMR, where the signal at 165.0 ppm is significantly enhanced (Fig. 4B).

FIGURE 3

The ^{13}C MAS NMR peak positions do not suffer any noticeable displacements after the material is reacted with H_2O_2 or subsequently heated (Fig. 4A). The C_i to C_e integrated area ratio of 1.0 is also constant for all of the tested samples (Table 2). It confirms that the bulk structure of PCN is retained and the relative quantity of the uncondensed units is also unchanged, in spite of the procedures the material underwent.

FIGURE 4

TABLE 2

One of the characteristic features of PCN is a strong hydrogen bonding of NH_2 and NH functionalities to N atoms of another heptazine [27,53]. There is still no consensus in the assignation of the most intense ^{1}H maximum in polymerised C_3N_4 heptazines. On the basis of theoretical calculations, it is suggested that the peak at about 4.3 ppm corresponds to the free amino-groups of PCN [54]. However, the alternative view, founded on the experimental data

collected from polymerised heptazine (melon), attributes it to the protons of hydrogen-bonded water molecules [53,55]. The decrease of the intensity of this maximum under *in-situ* heat treatment at 150 °C in NMR apparatus is in accord with the above hypothesis [56]. Although adsorbed water is not a part of the structural PCN unit, the type of its interaction with PCN gives information about the state of the surface species in the photocatalysts. A relatively narrow maximum, of 340 Hz of half-width at half-maximum (HWHM) of the H1 peak centred at approximately 4.5 ppm observed for the **TE** sample is noticeably broadened to 548 and 520 Hz for the **TEO** and **TEO200** samples, respectively. This could indicate the involvement of water adsorption sites in hydrogen bonding with other species present in PCN-H_2O_2 (Fig. 4C, Fig. S5A-C, Table 2). For **TEO300** and **TEO400** the corresponding HWHM value is reduced again (Fig. S5D,E, Table 2). This finding suggests that the modification of water adsorption sites in **TEO** and **TEO200** is due to the changes in the hydrogen bonding network caused by the attachment of hydrogen peroxide molecules to the amino-groups and heptazine nitrogen atoms (Fig. 3). On the other hand, **TEO400** having its melon layers well-separated and hydrogen bonding between them significantly reduced demonstrates a narrow peak at 4.5 ppm, which can be attributed to the adsorption of water molecules on well-defined surface sites.

The defect sites in PCN, i.e. NH_2 and NH species, according to Syefarth et al. [55], reveal themselves at 10 and 9.5 ppm, respectively, and a very similar range of chemical shifts, from 8.4 to 10.9, was also proposed by Hu et al [54]. (Fig. 3). On the ^{1}H MAS NMR spectrum of the **MHP** adduct, the main peak is centred at 10.9 ppm, and it can be assigned to the protons of H_2O_2 as well as to the developed hydrogen bonding in a melamine peroxosolvate crystal, where one molecule of H_2O_2 is able to interact with six melamine molecules [52] (Fig. S6). The much lower concentration of H_2O_2 in the PCN-H_2O_2 materials and interference of the protons of the NH– and NH_2–groups make it difficult to fully understand the contribution of this peak to the spectra. The deconvolution of the spectra by three Lorentz functions centred at about of 4.5 (H1), 9.4 (H2), and 1.0 (H3) ppm indicates that the peak at 9.4 ppm for the **TEO** and **TEO200** samples is significantly broadened and its contribution to the spectra is greater than for the other PCN samples (Fig. S5, Table 2). This finding can be attributed to the protons of H_2O_2 bonded to carbon nitride and to the displacement of the chemical shift maxima of the NH_2 moieties, due to the formation of hydrogen bonding between amino-groups and heptazine nitrogens mediating H_2O_2

(Fig. 3). The peak at approximately 1.0 ppm (H3) could be assigned to H_2O adsorbed on isolated basic sites of carbon nitride as it occurs on the surface of basic oxides [57].

Electronic structure

The band gap (BG) of the thermally etched carbon nitride (**TE**) is 2.76 eV (Fig. 5A, Table 1), which is close to the value reported earlier for the same type of photocatalysts [39]. The valence band (VB) of this sample is positioned at 1.59 eV, lower than that of the bulk PCN synthesised via the same process [38] (Fig. 5A inset, Table 1). The treatment of the thermally etched polymeric C_3N_4 with H_2O_2 does not change the BG value significantly, although a new absorption edge at lower energies of approximately 2.19 eV appears (Fig. 5B, Table 1). This could be explained by the formation of midgap states in the electronic structure of the PCN-H_2O_2 adduct, which is also deduced from the reduced value of its VB (Fig. 5B, inset). The heat treatment of **TEO** causes a slight decrease in the concentration of oxygen belonging to the bonded H_2O_2 (Table 1). Nevertheless, the absorption edge at 2.16 eV is retained (Fig. 5C, Table 1). Moreover, it is obvious that the sample undergoes some other changes, as its BG value decreases to 2.67 eV, while its VB has a potential of 1.52 eV (Fig. 5C inset, Table 1). Considering the evidenced by NMR studies strong hydrogen bonding in the **TEO** and **TEO200** samples, it can be hypothesised that the changes in their electronic structures are due to a strong interaction between adjacent carbon nitride units which interact with H_2O_2. The increase of thermal treatment temperature up to 300 °C results in an almost complete disappearance of the midgap absorption edge observed for the above discussed samples, and in the BG value equal to that of the parent material, **TE** (Fig. 5D, Table 1). Notably, the VB position maintains the same value of 1.52 eV (Fig. 5D inset, Table 1). The shift of the (002) diffraction maximum observed for **TEO400** (Fig. 1) could be related to its thermal etching at high temperatures in an oxidative atmosphere. Indeed, the increase of the BG and VB values is in accord with this hypothesis as the same effect of thermal etching on the BG was also observed elsewhere [39].

FIGURE 5

The PL spectra registered after the excitation at 365 nm show photoluminescence quenching for the PCN-H_2O_2 samples, which can be explained by the favoured charge separation on strongly

hydrogen bonded carbon nitride units. In addition, the appearance of a new PL band for the PCN-H_2O_2 adducts can be noticed (Fig. S7).

N_2 physisorption

All the prepared samples show the adsorption isotherms of IV type with a hysteresis loop of a mixed H3-H4 type corresponding to mesoporous materials with broad pore-size distribution (Fig. S8). The porous structure itself barely changes after the PCN-H_2O_2 adduct is formed and the subsequent thermal treatment is applied, however, the differences in SSA values are drastic (Fig. S8, Table 1). The SSA of **TEO** is reduced to 70 m^2 g^{-1} compared to 94 m^2 g^{-1} of **TE** (Table 1). The SSAs of **TEO200** and **TEO300** are smaller, i.e. 23 and 30 m^2 g^{-1}, respectively (Table 1, Fig. S8). It has already been proposed while discussing the XRD and DRS data that **TEO400** shows the features characteristic of thermally etched carbon nitride. Indeed, the increase of its SSA value up to 168 m^2 g^{-1} unambiguously confirms this supposition (Table 1. Fig. S8).

TPD-MS analysis of the PCN and PCN-H_2O_2 samples

The MS analysis of the volatile substances evolved during the thermal treatment of the **TE** and **TEO** samples under inert atmosphere shows the presence of 18 amu attributed to adsorbed or chemically bonded H_2O in PCN (Fig. S9A). For the **TE** sample water removal ends at about 200 °C, while the additional smaller peak observed for **TEO** around 300 °C could be due to H_2O formed in the result of the bonded H_2O_2 decomposition (Fig. S9A inset). The materials release CO_2 (44 amu) at different temperatures that might be attributed to the modification of the basic adsorption surface sites in the PCN-H_2O_2 or to the release of O_2 during the PCN-H_2O_2 heating, which can partially oxidise surface carbon nitride species (Fig. S9B). Three more gaseous products with mass numbers 32, 30, and 28 amu, respectively assigned to O_2, NO, and N_2, are detected only for the **TEO** sample (Fig. S9C-E). These species are produced as a result of the bonded H_2O_2 decomposition and the oxidation of the surface carbon nitride groups (Fig. S9C-E). The findings corresponding to the O_2 and N_2 generation during the adduct decomposition are consistent with the proposed thermal degradation pathway of another H_2O_2 complex compound urea-hydrogen peroxide adduct [58]. Summarizing, the PCN-H_2O_2 is likely to contain a weakly bonded hydrogen peroxide, which decomposes at temperatures below 200 °C producing H_2O and

O_2 but also strongly bonded peroxo species, whose thermal degradation gives rise to oxidation of the surface $C–NH_x$-groups producing gaseous NO, CO_2 and N_2.

HMF partial photo-oxidation to FDC under UV-irradiation

The adsorption capacity of the photocatalysts did not exceed 1% of the initial HMF concentration. Photolyses of the substrate and of the principal reaction product were determined for the used photocatalytic set-up earlier [39]. The possible release of H_2O_2 by the PCN-H_2O_2 photocatalysts into water suspensions was tested. No H_2O_2 was found in the aqueous suspension of photocatalysts when it was heated up to 50 °C, while negligible quantities, not exceeding 6.6 μmol of H_2O_2 per 1 g of the PCN-H_2O_2 adduct, were released at boiling point.

FIGURE 6

Expectedly, under UV irradiation the thermally etched PCN (**TE**) shows high HMF conversion approaching 47%, which is close to that reported elsewhere [39]. Also, it is the most active sample among all the tested ones (Fig. 6A, Table 3). The treatment of **TE** with hydrogen peroxide results in almost three times less active photocatalyst (**TEO**), due probably to its reduced SSA (70 m^2 g^{-1}) (Fig. 6A, Table 3) and to the blockage of certain carbon nitride surface sites to which H_2O_2 is attached. Despite the further reduction of the SSA observed for the thermally treated PCN-H_2O_2 adducts at 200 °C (**TEO200**) and 300 °C (**TEO300**), the HMF conversion degree barely changes (Fig. 6A). The explanation of this finding could be found in the improved charge transfer and charge separation occurring on strongly hydrogen bonded melon units. The activity of the **TEO400** sample, however, was found higher than that of **TEO300**, but still less significant than that of **TE** (Fig. 6A). Although the SSA of **TEO400** is the highest among all of the tested materials, this property does not exclusively determine the photocatalytic performance of carbon nitride materials. Considering other differences in the **TE** and **TEO400** features, the only one able to explain the decreased photoactivity is the low surface oxygen content and lower O 1s binding energy value of the latter (Table 1). It might be an indication of a higher strength of **TEO400** basic sites, hence the presence of strongly bonded adsorbed oxygen species [59], whose removal from the surface in a form of radicals is hindered.

TABLE 3

The highest amount of FDC produced during the photocatalytic HMF conversion was observed for the **TE** sample, while for **TEO300** this value was the lowest one (Fig. 6B, Table 3). Despite the reduced conversion degree, **TEO** demonstrates significantly improved selectivity for the FDC production reaching 71% at 20% of HMF conversion, while the corresponding value for the thermally etched PCN is only 40% (Table 3, Fig. 6C). Moreover, the selectivity is also maintained on a nearly the same level throughout the reaction (Fig. 6C). Subjecting the PCN-H_2O_2 adduct to thermal treatment at 200 °C (**TEO200**) does not affect the selectivity to FDC formation (Fig. 6C). For the **TEO300** and **TEO400** samples, the selectivity is very similar to that of **TE** (Fig. 6C). This can be attributed to the drop in the content of oxygen corresponding to the presence of H_2O_2 in the PCN-H_2O_2 adduct (Table 1). The relation of selectivity to FDC formation versus HMF conversion represented in Figure 6D indicates that the PCN-H_2O_2 adduct samples have higher selectivity to FDC production at the same conversion extent than **TE**, **TEO300** and **TEO400** (Table 3). For the **TEO** and **TEO200** photocatalysts, similar values of the rates of HMF conversion and FDC formation are obtained, indicating that HMF to FDC oxidation is the primary process occurring in the irradiated suspension (Table 3). For the other materials (**TE**, **TEO300**, **TEO400**) the respective values differ by more than a factor of 2 because parallel reactions take place (Table 3). There are several factors responsible for HMF to FDC selectivity being below 100 %. Once FDC is produced in the reaction suspension, it is slowly photolysed to FFA (Fig. S10). Another factor contributing to the selectivity loss, especially in case of the **TE**, **TEO300** and **TEO400** samples, is the direct oxidation of HMF to aliphatic carboxylic acids, detected but not identified in the present work.

The sample prepared by the thermal etching of the PCN-H_2O_2 adduct at 450 °C (**TEO450**) has also been studied. Although it shows an HMF conversion degree higher than that of **TE**, it does not demonstrate any improvement of the selectivity (Fig. S11). The alternative method of H_2O_2-modification via refluxing the suspension of H_2O_2 and **TE** resulted in the formation of the **TEO_R** photocatalyst having mild reaction rate and selectivity of about 60%, which is lower than that observed for **TEO** (Fig. S11).

The recoverability of the **TEO** photocatalyst was tested in three consecutive reaction cycles under UV irradiation. **TEO** maintains the same conversion degree and the selectivity to FDC formation

equal to 19-21% and 68-82%, respectively, thus proving itself as an efficient photocatalyst for the partial photo-assisted HMF oxidation (Fig. S12).

HMF partial photo-oxidation to FDC under solar light

PCN is an attractive photocatalyst for reactions occurring under solar light, due to the electronic structure which allows its activation under visible-light irradiation. Unsurprisingly, the reaction rate under sunlight is significantly improved for all of the tested materials with respect to that achieved under the UV lamps, which is attributed to the higher UV photon flux of the outdoor irradiation (Fig. 7A, Table 3). The most active **TE** sample is capable of oxidising almost all of the substrate within the reaction time, while other photocatalysts show degrees of conversion nearly twice increased with respect to those obtained under the UV-source used (Fig. 7A, Table 3). The comparison of the cumulative energies entering the UV and solar-light reactors shows that the photocatalytic activity is almost directly proportional to the energy of irradiation with wavelengths from 315 to 400 nm (Table 3). However, the performance of **TEO200** stands aside of the common trend, which is most probably due to its narrower BG with respect to those of the other tested photocatalysts (Fig. 7A, Table 3). The concentration of FDC, for the **TE** and **TEO400** samples, increases with the cumulative energy up to about 1.65 kJ, after which a plateau is observed (Fig. 7B). This finding can be explained by considering the high extent of conversion achieved in the presence of these samples because the product itself becomes a target for photo-produced radical species after most of the substrate is oxidised. As far as the selectivity is concerned, no significant differences can be noticed between the results obtained under UV irradiation and solar light (Fig. 7C). The selectivity toward FDC approaches 100% at low HMF conversion values in the presence of the **TEO** sample, while it ranges between 70 to 80% for moderate and high conversions in the cases of the **TEO** and **TEO200** samples. These figures are higher than the corresponding ones attained by the thermally etched PCN (**TE**), **TEO300** and **TEO400** samples (Fig. 7D).

FIGURE 7

Additional tests to prove the effectiveness of the **TEO** sample for the conversion of HMF to FDC at enhanced concentrations of the substrate (1 and 2 mM) were performed. The quantity of HMF converted is found to be in a nearly direct dependency from the initial HMF concentration (Fig.

8A). **TEO** converts 15.6 μmol of HMF when the initial substrate concentration is 0.5 mM, while 30.5 and 56.3 μmol are converted when the initial concentrations are 1.0 and 2.0 mM, respectively (Fig. 8A). Figure 8B shows that the selectivity to FDC decreases by increasing HMF initial concentration (Fig. 8B), however, it appears to be on the same level when plotted against the quantity of HMF reacted (Fig. 8C).

FIGURE 8

A dramatic effect on the selectivity of the photo-oxidation of HMF to FDC, consequent to the formation of the PCN-H_2O_2 adduct, could be attributed to the type of interaction of the substrate molecules with some carbon nitride surface sites. In a previous study on the HMF photo-oxidation in the presence of thermally exfoliated PCN, the selectivity to FDC up to 75% was obtained in the organic solvent [39], and this value is close to that found in the present work for the PCN-H_2O_2 adducts in aqueous medium. The presence of water could have a detrimental effect on the reaction selectivity. Indeed, the test for hydroxyl radicals generation by TA method confirms their formation, and in particular that **TE** produces higher quantities of $^\bullet$OH than **TEO** (Fig. S13). It is commonly accepted that PCN cannot form $^\bullet$OH radicals by directly oxidising water with photo-generated holes, whilst it is possible by the action of photo-generated electrons mediating H_2O_2 formation [60]. Nonetheless, we have not observed the photocatalytic production H_2O_2 in the absence of the substrate. Another pathway could also be considered: the non-polymerised C_3N_4 species bearing Brønsted basic sites, i.e. amino-groups, form hydrogen bonds in water suspension, giving positively charged -NH_3^+ surface moieties [61] (Fig. 9A). The coordination of water in this way allows it being attacked by the photo-generated holes ripping off electrons from the H_2O molecules and forming $^\bullet$OH radicals, which are not produced on the polymerised aromatic units of carbon nitride, due to the low potential of its VB [28] (Fig. 9A). For the thermally etched PCN photocatalyst, the NH_2 functionalities, where the produced $^\bullet$OH radicals are localized, are accessible for the interaction with HMF, which can be attached to the uncondensed carbon nitride species in a similar way as it was proposed for an aromatic compound [41]. The reaction of HMF with hydroxyl radical leads to the ring opening and the formation of aliphatic intermediates, observed but not studied in this work, thus reducing the selectivity of the photo-oxidation reaction toward the formation of FDC (Fig. 9B). On the other hand, H_2O_2 blocks the amino-groups of the PCN-H_2O_2 adducts, thus creating a steric hindrance for the HMF molecule interaction with the

carbon nitride surface sites (Fig. 9C). Therefore, the PCN-H$_2$O$_2$ samples favour higher selectivity to FDC formation, whilst the HMF conversion rates appear lower, due to the absence of hydroxyl radicals action and to the smaller SSAs of these photocatalysts (Fig. 9C).

FIGURE 9

Conclusions

PCN reacts with H$_2$O$_2$ producing PCN-H$_2$O$_2$ adduct stable up to 200 °C in air. The formed material does not release H$_2$O$_2$ into the suspension in aqueous medium and under irradiation, thus ensuring its usability for photocatalytic applications. The result of H$_2$O$_2$ bonding to the carbon nitride partially polymerised and non-polymerised sites is the development of hydrogen bonding network within the material. The formation of the adduct is also responsible for the blockage of NH$_2$ functional groups, which are detrimental for the selective partial photocatalytic oxidation of HMF to FDC. The bonded H$_2$O$_2$ creates a steric hindrance for the HMF interaction with amino-groups, where ˙OH radicals, driving to furanic ring opening and hence unselective oxidation of the substrate, are probably localized. The elimination from the reaction process of the pathway involving the action of hydroxyl radicals leads to the enhancement of the selectivity toward the FDC production under outdoor illumination from 45% to 88% at 20% of HMF conversion. Moreover, the prepared PCN-H$_2$O$_2$ adduct photocatalyst proved itself recoverable and efficient in the solar light assisted conversion of HMF even at high initial concentrations of the substrate. The present work has underlined the importance of the modification of the surface species of PCN for its improved performance in partial photo-oxidation reactions.

Conflicts of interest

There are no conflicts to declare.

Acknowledgements

Notes and references

1   S. Suganuma, K. Nakajima, M. Kitano, D. Yamaguchi, J. Am. Chem. Soc. 130 (2008) 12787-12793.

2   J.N. Chheda, Y. Roman-Leshkov, J.A. Dumesic, Green Chem. 9 (2007) 342-350.

3   G.Z. Papageorgiou, D.G. Papageorgiou, Z. Terzopoulou, D.N. Bikiaris, Eur. Polym. J., 83 (2016) 202-229.

4   A.F. Sousa, C. Vilela, A.C. Fonseca, M. Matos, C.S.R. Freire, G.-J.M. Gruter, J.F.J. Coelho, A.J.D. Silvestre, Polym. Chem. 6 (2015) 5961-5983.

5   I. Delidovich, P.J.C. Hausoul, L. Deng, R. Pfützenreuter, M. Rose, R. Palkovits, Chem. Rev. 116 (2016) 1540-1599.

6   A.S. Amarasekara, D. Green, L.D. Williams, Eur. Polym. J. 45 (2009) 595–598.

7   T. Xiang, X. Liu, P. Yi, M. Guo, Y. Chen, C. Wesdemiotis, Y. Pang, Polym. Int. 62 (2013) 1517-1523.

8   J.M.R. Gallo, D.M. Alonso, M.A. Mellmer, J.A. Dumesic, Green Chem. 15 (2013) 85-90.

9   X. Tong, Y. Ma, Y. Li, Appl. Catal. A: Gen. 385 (2010) 1-13.

10 I. Sadaba, Y.Y. Gorbanev, S. Kegnæs, S. Reddy, ChemCatChem. 5 (2013) 284-293.

11 C. Carlini, P. Patrono, A. Maria, R. Galletti, Appl. Catal. A: Gen. 289 (2005) 197-204.

12 J. Nie, J. Xie, H. Liu, J. Catal. 301 (2013) 83-91.

13 F. Neat, N. Petrea, R. Petre, V. Somoghi, M. Florea, V.I. Parvulescu, Catal. Today. 278 (2016) 66-73.

14 M. Chatterjee, T. Ishizaka, A. Chatterjee, H. Kawanami, Green Chem. 19 (2017) 1315-1326.

15 Y. Shiraishi, T. Hirai, J. Photochem. Photobiol. C: Photochem. Rev. 2008, 9, 157-170.

16 X. Lang, W. Ma, C. Chen, H. Ji, J. Zhao, Acc. Chem. Res. 47 (2014) 355-363.

17 V. Augugliaro, G. Camera-roda, V. Loddo, L. Palmisano, J. Soria, S. Yurdakal, J. Phys. Chem. Lett. 6 (2015) 1968-1981.

18 G. Palmisano, A. Albini, G. Marcì, L. Palmisano, D. Ravelli, RSC Energy Environ. Series. 15 (2016) 303.

19 X. Lang, J. Zhao, Chem Soc Rev. 43 (2014) 473-486.

20 J. Kou, C. Lu, J. Wang, Y. Chen, Z. Xu, R.S. Varma, Chem. Rev. 117 (2017) 1445-1514.

21 D.W. Wakerley, M.F. Kuehnel, K.L. Orchard, K.H. Ly, T.E. Rosser, E. Reisner, Nature Energ. 2 (2017) 17021.

22 S.-H. Li, S. Liu, J.C. Colmenares, Y.-J. Xu, Green Chem., 18 (2016) 594-607.

23 G. Chatel, S. Valange, R. Behling, J.C. Colmenares, ChemCatChem. 9 (2017) 2615-2621.

24 L. Ozcan, P. Yalcin, O. Alagoz, S. Yurdakal, Catal. Today. 281 (2017) 205-213.

25 S. Yurdakal, B. S. Tek, O. Alagöz, V. Augugliaro, V. Loddo, G. Palmisano, L. Palmisano, ACS Sustain. Chem. Eng. 1 (2013) 456-461.

26 I. Krivtsov, M. Ilkaeva, E. Salas-Colera, Z. Amghouz, J.R. García, E. Díaz, S. Ordoñez, S. Villar-Rodil, J. Phys. Chem. C. 121 (2017) 6770-6780.

27 F.K. Kessler, Y. Zheng, D. Schwarz, C. Merschjann, W. Schnick, X. Wang, M.J. Bojdys, Nature Mater., 2017, 17030.

28 X. Wang, K. Maeda, A. Thomas, K. Takanabe, G. Xin, J.M. Carlsson, K. Domen, M. Antonietti, Nat. Mater. 8 (2008) 76-80.

29 X. Dai, M. Xie, S. Meng, X. Fu, S. Chen, Appl. Catal. B: Environ. 158-159 (2014) 382-390.

30 F. Su. S. C. Mathew, G. Lipner, X. Fu, M. Antonietti, S. Blechert, X. Wang, J. Am. Chem. Soc. 123 (2010) 16299-16301.

31 J. Xu, L. Luo, G. Xiao, Z. Zhang, H. Lin, X. Wang, J. Long, ACS Catal. 4 (2014) 3302-3306.

32 S. Verma, R.B.N. Baig, M.N. Nadagouda, R.S. Varma, ACS. Sustain. Chem. Eng. 4 (2016) 1094-1098.

33 X. Chen, J. Zhang, X. Fu, M. Antonietti, X. Wang, J. Am. Chem. Soc.. 131 (2009) 11658-11659.

34 X.-H. Li, X. Wang, M. Antonietti, ACS Catal. 2 (2012) 2082-2086.

35 X.-H. Li, J.-S. Chen, X. Wang, J. Sun, M. Antonietti, J. Am. Chem. Soc. 133 (2011) 8074-8077.

36 Z. Ding, X. Chen, M. Antonietti, X. Wang, ChemSusChem. 4 (2011) 274-281.

37   B. Long, Z. Ding, X. Wang, ChemSusChem. 6 (2013) 2074-2078.

38   M. Bellardita, E.I. García-López, G. Marcì, I. Krivtsov, J.R. García, L. Palmisano, Appl. Catal. B: Environ. 220 (2018) 222-233.

39   I. Krivtsov, E.I. García-López, G. Marcì, L. Palmisano, Z. Amghouz, J.R. García, E. Díaz, S. Ordóñez, Appl. Catal., B: Environ. 204 (2017) 430-439.

40   A. Akhundi, E.I. García-López, G. Marcì, A. Habibi-Yangjeh, L. Palmisano, Res. Chem. Intermed. 43 (2017) 5153-5168.

41   M. Ilkaeva, I. Krivtsov, E.V. Bartashevich, S. Khainakov, J.R. García, E. Díaz, S. Ordóñez, Green Chem. 19 (2017) 4299-4304.

42   K. Wang, Q. Li, B. Liu, B. Cheng, W. Ho, J. Yu, Appl. Catal. B: Environ. 176–177 (2015) 44-52.

43   P. Niu, L. Zhang, G. Liu, H.-M. Chen, Adv. Funct. Mater. 22 (2012) 4763-4770.

44   V. Augugliaro, E.I. García-López, V. Loddo, S. Malato-Rodriguez, I. Maldonado, G. Marcì, R. Molinari, L. Palmisano, Solar Energy. 79 (2005) 402-408.

45   T. Hirakawa, Y. Nosaka, Langmuir, 18 (2002) 3247-3254.

46   S. Liu, D. Li, H. Sun, H. Ming, M. O. Tadé, S. Wang, J. Colloid Interface Sci., 468 (2016) 176-182.

47   J. Li, B. Shen, Z. Hong, B. Lin, B. Gao, Y. Chen, Chem. Comm. 4 (2012) 12017-12019.

48   F. Dong, Y. Li, Z. Wang, W. Ho, Appl. Surf. Sci. 358 (2015) 393-403.

49   B. Marchon, J. Carrazza, H. Heinemann, G. A. Somorjai, Carbon. 26 (1988) 507-514.

50   T. Nagaishi, M. Matsumoto, S. Yoshigana, J. Therm. Anal. Calorim. 36 (1990) 55-60.

51   G. Chehardoli, M.A. Zolfigol, Phosphorus, Sulfur Silicon Relat. Elem. 185 (2010) 193-203.

52   I.Yu. Chernyshov, M.V. Vener, P.V. Prikhodchenko, A.G. Medveddev, O. Lev, A.V. Churakov, Cryst. Growth Des. 17 (2017) 214-220.

53   L. Seyfarth, J. Senker, *Phys.* Chem. Chem. Phys. 11 (2009) 3522-3531.

54   Y. Hu, Y. Shim, J. Oh, S. Park, S. Park, Y. Ishii, Chem. Mater. 29 (2017) 5080-5089.

55   L. Seyfarth, J. Seyfarth, B. V. Lotsch, W. Schnick, J. Senker, Phys. Chem. Chem. Phys. 12 (2010) 2227-2237.

56   W.J. Gammon, G.L. Hoatson, B.C. Holloway, R.L. Vold, A.C. Reilly, Phys. Rev. B. 68 (2003) 195401.

57 M.A. Aramendía, J.A. Benítez, V. Borau, C. Jiménez, J.M. Marinas, J.R. Ruiz, F. Urbano, Langmuir. 15 (1999) 1192-1197.

58 R. Matyas, J. Selesovsky, V. Pelikan, M. Szala, S. Cudzilo, W. A. Trzcinsky, M. Gozin, Propellant. Explosiv. Pyrotech. 42 (2017) 198-203.

59 E. Díaz, E. Muñoz, A. Vega, S. Ordóñez, Ind. Eng. Chem. Res. 47 (2008) 412-418.

60 J. Liu, T. An, Z. Chen, Z. Wang, H. Zhou, T. Fan, D. Zhang, M. Antonietti, J. Mater. Chem. A. 5 (2017) 8933-8938.

61 S. Li, K. Su, Z. Li and B. Cheng, Green Chem. 18 (2016) 2122-2128.

Figure captions

Figure 1. XRD patterns of the prepared PCN and PCN-H_2O_2 samples.

Figure 2. XPS spectra of O 1s region of the PCN and PCN-H_2O_2 samples.

Figure 3. Proposed model of interactions in the PCN-H_2O_2 adduct.

Figure 4. (A) ^{13}C MAS NMR, (B) ^1H-^{13}C CPMAS NMR and (C) ^1H MAS NMR spectra of the PCN and PCN-H_2O_2 samples.

Figure 5. DR spectra and XPS VB spectra (inset) of (A) **TE**, (B) **TEO**, (C) **TEO200**, (D) **TEO300**, and (E) **TEO400**.

Figure 6. (A) HMF and (B) FDC concentrations and (C) selectivity to FDC formation versus reaction time; (D) selectivity to FDC versus HMF conversion for the prepared photocatalysts under UV irradiation.

Figure 7. (A) HMF and (B) FDC concentrations and (C) selectivity to FDC formation versus reaction time; (D) selectivity to FDC versus HMF conversion for the prepared photocatalysts under solar light irradiation.

Figure 8. (A) HMF reacted and (B) selectivity to FDC versus cumulative energy; (C) selectivity to FDC formation versus amount of HMF reacted in the presence of the **TEO** photocatalyst under solar light irradiation at varying initial HMF concentrations.

Figure 9. (A) Hypothetical mechanism of hydroxyl radical formation on PCN basic sites; (B) proposed types of interaction and photo-oxidation of HMF on PCN, and (C) on PCN-H_2O_2.

Tables

Table 1. XPS data, electronic structure and SSA values of the PCN and PCN-H$_2$O$_2$ samples

Sample	XPS surface composition [at%]	O 1s peak position [eV]	BG [eV]	VB [eV]	CB [eV]	SSA [m^2 g^{-1}]
TE	C$_{42.3}$N$_{54.4}$O$_{3.3}$	532.5	2.76	1.59	-1.17	94
TEO	C$_{40.8}$N$_{53.8}$O$_{5.4}$	531.6	2.74/2.19	1.44	-1.30	70
TEO200	C$_{39.6}$N$_{55.8}$O$_{4.6}$	531.6	2.67/2.16	1.52	-1.15	23
TEO300	C$_{41.0}$N$_{56.6}$O$_{2.4}$	531.5	2.72	1.52	-1.20	30
TEO400	C$_{41.7}$N$_{55.8}$O$_{2.5}$	532.3	2.81	1.65	-1.16	168
MHP		531.3				

Table 2. Solid state MAS NMR data obtained for the PCN and PCN-H$_2$O$_2$ samples

Samples	^{13}C MAS NMR C$_i$/C$_e$ ratio	Position of H1 peak [ppm]	HWHM of H1 maximum [Hz]	HWHM of H2 maximum [Hz]	^{1}H MAS NMR H2/H1 ratio
TE	1.02	4.5	340	1100	0.63
TEO	0.96	4.3	548	1624	1.06
TEO200	1.00	4.1	520	1888	1.91
TEO300	0.99	4.0	368	748	0.30
TEO400	1.00	4.5	196	904	0.45

Table 3. HMF initial conversion rate (r) under UV irradiation, HMF conversion and selectivity values under UV and natural solar light irradiation

Sample	UV				Natural solar light				Selectivity at 20% of HMF conversion [%]	
	Initial HMF conversion rate·10^2 [mM min^{-1}]	Initial FDC formation rate·10^2 [mM min^{-1}]	0.99 kJ (4 h)		0.99 kJ (~ 2 h)		1.8 kJ (~ 4 h)		UV	Natural solar light
			HMF Conversion [%]	Selectivity to FDC [%]	HMF Conversion [%]	Selectivity to FDC [%]	HMF Conversion [%]	Selectivity to FDC [%]		
TE	0.130	0.058	47	38	47	40	74	31	40	45
TEO	0.047	0.036	21	71	21	88	37	83	71	88
TEO200	0.037	0.029	20	75	30	77	51	75	75	73
TEO300	0.040	0.016	20	48	16	52	33	46	47	50
TEO400	0.069	0.021	28	43	34	42	58	35	46	44
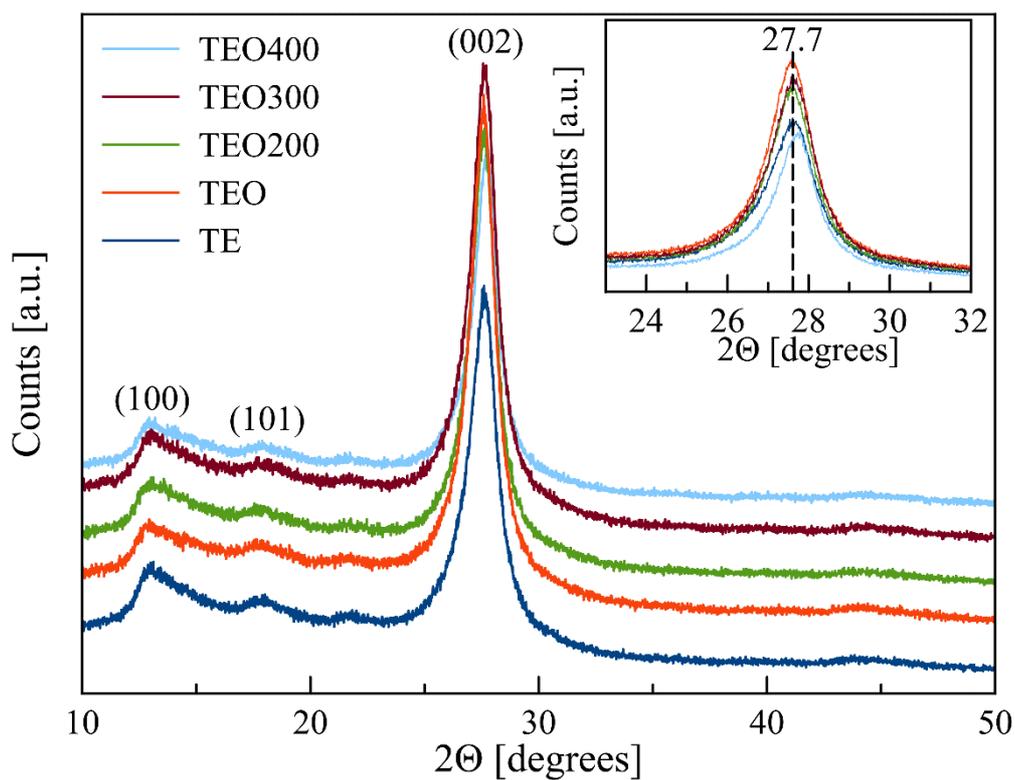
Fig. 1
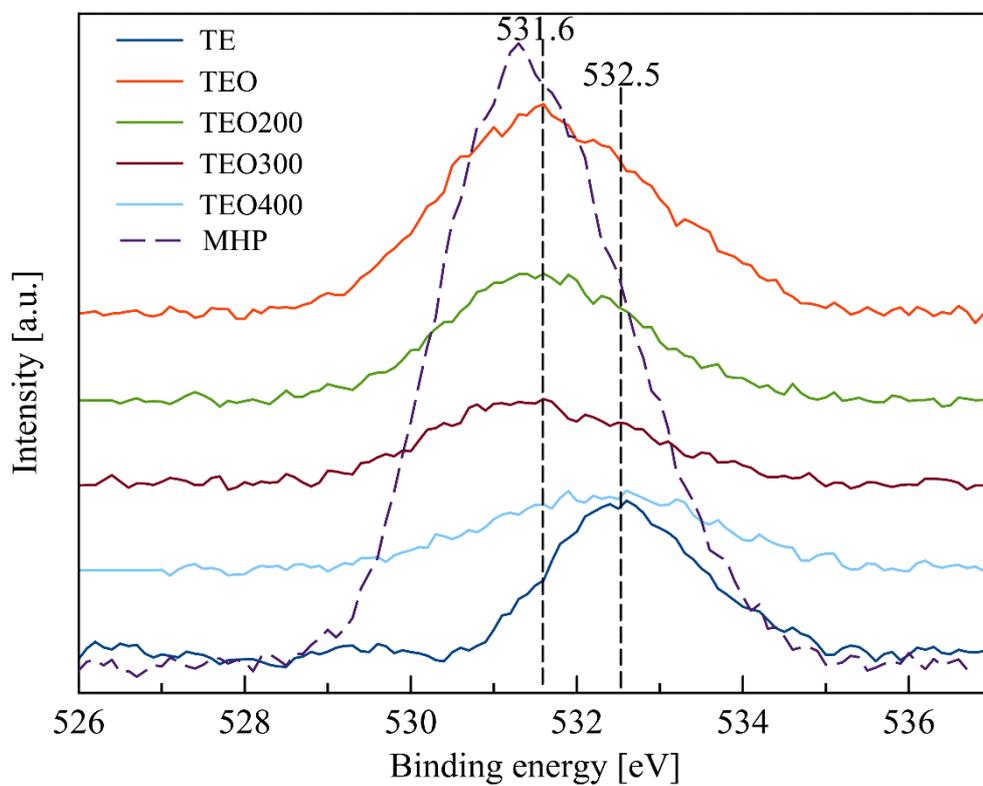
Fig. 2
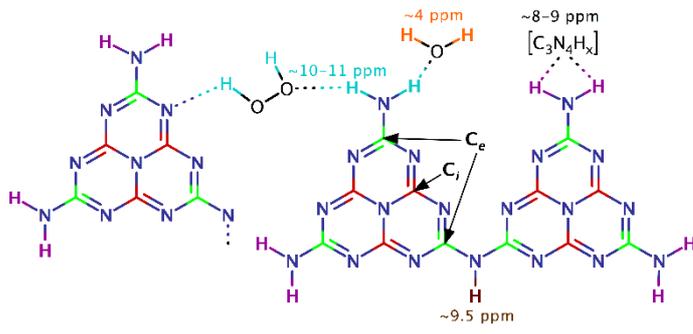
Fig. 3
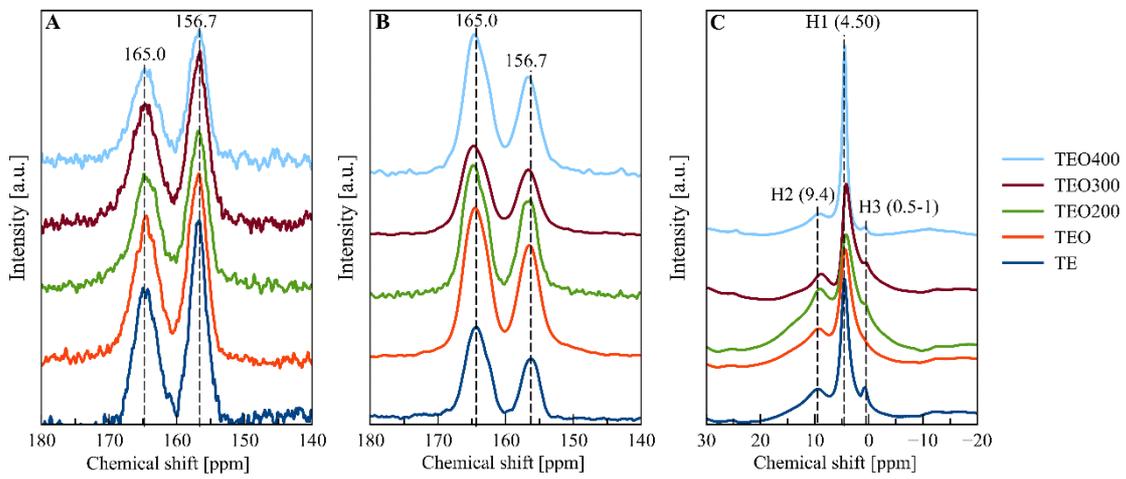
Fig. 4

Fig. 5

Fig. 6

Fig. 7

Fig. 8

Fig. 9